CrossMark

RESEARCH ARTICLE

Analysis of numerical simulations and influencing factors of seasonal manganese pollution in reservoirs

Hui Peng[1,2] · Xilai Zheng[1] · Lei Chen[3] · Yang Wei[1]

Abstract Seasonal manganese pollution has become an increasingly pressing water quality issue for water supply reservoirs in recent years. Manganese is a redox-sensitive element and is released from sediment under anoxic conditions near the sediment–water interface during summer and autumn, when water temperature stratification occurs. The reservoir water temperature and water dynamic conditions directly influence the formation of manganese pollution. Numerical models are useful tools to quantitatively evaluate manganese pollution and its influencing factors. This paper presents a reservoir manganese pollution model by adding a manganese biogeochemical module to a water quality model—CE-QUAL-W2. The model is applied to the Wangjuan reservoir (Qingdao, China), which experiences manganese pollution during summer and autumn. Field data are used to verify the model, and the results show that the model can reproduce the main features of the thermal stratification and manganese distribution. The model is used to evaluate the manganese pollution process and its four influencing factors, including air temperature, water level, wind speed, and wind directions, through different simulation scenarios. The results show that all four factors can influence manganese pollution. High air temperature, high water level, and low wind speed aggravate manganese pollution, while low air temperature, low water level, and high wind speed reduce manganese pollution. Wind that travels in the opposite direction of the flow aggravates manganese pollution, while wind in the same direction as the flow reduces manganese pollution. This study provides useful information to improve our understanding of seasonal manganese pollution in reservoirs, which is important for reservoir manganese pollution warnings and control.

Keywords Reservoir · Manganese pollution · Numerical simulation · Water temperature stratification

✉ Xilai Zheng
zhxilai@ouc.edu.cn

1   Key Laboratory of Marine Environment and Ecology, Ministry of Education, Ocean University of China, Qingdao 266100, China

2   State Key Laboratory of Simulation and Regulation of River Basin Water Cycle (SKL-WAC), China Institute of Water Resources and Hydropower Research (IWHR), Beijing 100038, China

3   School of Environmental Science and Engineering, Qilu University of Technology, Jinan 250353, China

Introduction

Pollution in drinking water reservoirs is a serious water safety issue worldwide. Manganese is a contaminant that is difficult to remove within the water treatment industry (Gantzer et al. 2009). Manganese is the second most abundant transition metal and exists in fresh water, seawater, sediments, and various kinds of minerals. Manganese is a redox-sensitive element that exists in three oxidation states: II, III, and IV (Atkinson et al. 2007; Graham et al. 2012). This element tends to remain in a reduced form in the water, particularly under anoxic conditions (dissolved oxygen (DO) <16 % of saturation; Baden et al. 1995). Manganese in water sources can cause significant harm to human health and industrial production (Kohl and Medlar 2006). The World Health Organization (World Health Organisation 2011) and Chinese drinking water quality standards recommend manganese values of 0.1 mg/l.

Many reservoirs worldwide have reported manganese pollution (Löfgren and Boström 1989; Johnson et al. 1991; Hamilton-Taylor et al. 1996; Miao et al. 2006; Gantzer et al.

2009; Abesser et al. 2010; Bryant et al. 2011). No external manganese source was involved with most of these reservoirs, and manganese pollution occurred during summer and autumn. Previous studies showed that seasonal manganese pollution comes from sediment (Farmer and Lovell 1984; Bryant et al. 1997). The release of manganese from sediment is related to the anoxic conditions near the sediment–water interface (Gantzer et al. 2009).

Previous studies of manganese in reservoirs have found that seasonal temperature stratification is the main trigger of summer reservoir manganese pollution (Zaw and Chiswell 1999). During summer, the position of the Mn redox boundary changes from the sediments to the water column because of water temperature stratification (Bryant et al. 2011). This phenomenon can induce the diffusion of Mn(II) from the sediment pore water into the overlying water (Sakata 1985; Sundby et al. 1986; Atkinson et al. 2007; Pakhomova et al. 2007; Graham et al. 2012). High concentrations of manganese appear in the hypolimnion of reservoirs. During autumn, the water temperature is vertically equal, and water column overturning induces oxidation in the entire water column. Thus, Mn(II) in the water is oxidized into manganese oxide and settles onto sediments, and manganese pollution disappears (Kristiansen et al. 2002).

Reservoir water temperature and water dynamic conditions directly influence the formation and distribution of manganese pollution (Stauffer 1993; Roitz et al. 2002). Environmental factors such as air temperature, wind speed, wind direction, and the depth of the water can affect the water temperature and dynamics, thereby influencing the manganese pollution in reservoirs. Improving our understanding of the influence from environmental factors is useful to prevent and control the seasonal manganese pollution. Previous studies that examined the influencing factors of manganese pollution included field or laboratory tests in the microenvironment near the water–sediment interface. Graham et al. (2012) investigated the distribution of manganese and its association with large organic colloids. Abesser et al. (2010) studied the mobilization of iron and manganese from sediments in a Scottish Upland reservoir. Atkinson et al. (2007) tested the effect of the overlying water's pH, dissolved oxygen, salinity, and sediment disturbances on manganese release from sediments by laboratory tests. Few analyses have studied the environmental factors of the entire reservoir; because manganese pollution involves complex hydrodynamic and water quality processes, field monitoring and laboratory testing have difficulty accurately describing all these processes.

Numerical models can be used to quantitatively study manganese pollution. Moreover, models can provide a useful method to analyze the impact of different environmental factors. Manganese pollution models include water dynamic, thermal, transport, chemical, and biological processes to represent the generation and migration of manganese pollution. However, only a few water quality models or geochemical models have manganese pollution functions, including Johnson et al. (1991), who used a vertical one-dimensional manganese circulation model to simulate manganese cycles in seasonal hypoxia lakes, and Lopes et al. (2010), who conducted vertical one-dimensional biogeochemical reaction simulations in both the sediments and water in Aydat Lake. However, their models were one-dimensional models and could not display the entire reservoir. Castelletti et al. (2010) used ELCOM to simulate the effects of aerations on manganese elimination. ELCOM is a three-dimensional model that can simulate manganese in an entire reservoir. However, ELCOM and other three-dimensional models have rarely been applied to manganese pollution processes or the impact of environmental factors.

The objectives of this study were to (1) develop a manganese pollution model, (2) analyze the generation and migration of manganese pollution, and (3) discuss influencing factors such as the temperature, water level, wind speed, and wind direction in terms of their influence on manganese pollution. This study offers scientific support for reservoir manganese pollution warning and management and promotes the integrated management of water quantity, water quality, and water ecological environments.

Study site

The Wangjuan reservoir is located in the upstream portion of the Lianyin River in Qingdao, China. Its geographical position is 120° 34′ E–120° 37′ E, 36° 27′ N–36° 29′ N (as shown in Fig. 1). The reservoir was constructed in 1960 as a multifunctional reservoir for flood control, irrigation, and urban water supply.

The reservoir is located in a northern temperate coastal area, and the weather exhibits significant maritime climate characteristics. The climate is warm and rainy during summer, dry and evaporative during autumn, and windy and cold during winter. The annual average temperature is 12 °C, the average wind speed is 2.2 m/s, and the average precipitation is 635 mm. The intra-annual and inter-annual variety in precipitation is significant, and precipitation during the flood season (June–September) comprises approximately 70 % of the annual precipitation.

The catchment area of the reservoir is 72 km^2. The average water depth of the reservoir is 6.8 m, the average annual inflow is 12.2 million m^3, and the total storage capacity is 34.6 million m^3. The catchment is a hilly terrain that tilts from south to north. The length of the river upstream of the reservoir is 14.1 km, with a gradient of 0.0025. The catchment is 4.9 km wide on average and 9.1 km long.

Fig. 1 Location of the Wangjuan reservoir (Chen et al. 2015)
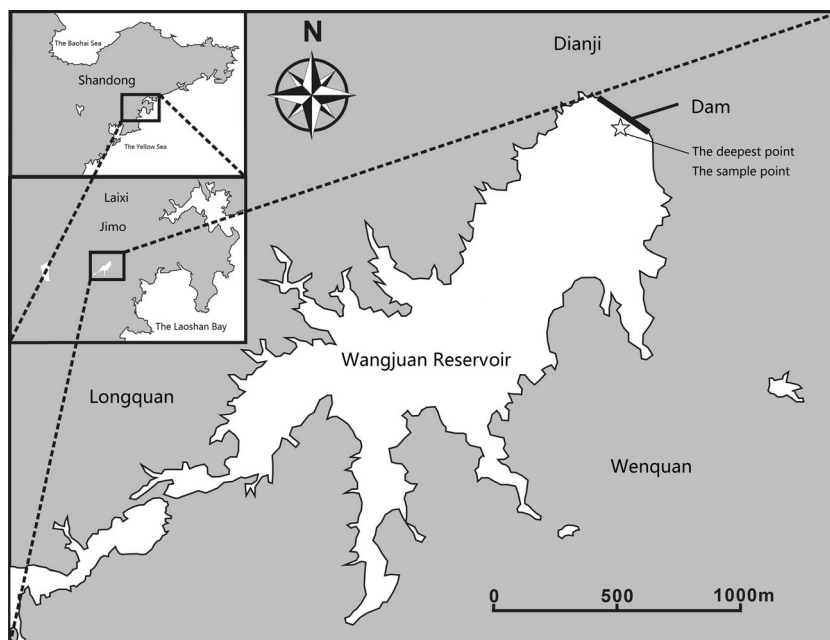
The areas to the northwest, southwest, and southeast of the catchment are mountainous and hilly, with bare rock and steep terrain. The landform consists of eroded tectonic and piedmont pluvial geomorphic surfaces. The bedrock is Cretaceous tuff from the Laiyang group, volcanic breccia, and argillaceous sandstone.

The daily water supply capacity of the reservoir is 40,000 m^3, and the annual water supply is approximately 7 million m^3. The check level is 48.30 m, and the design flood level is 47.56 m. The utilizable level and capacity are 44.90 m and 21.8 million m^3, respectively, while the dead level and capacity are 31.03 m and 440,000 m^3, respectively. Buildings include a dam, a spillway, a convey tunnel, and an emergency spillway.

The Wangjuan reservoir is an important urban drinking water source for the region, but the manganese in its drawing water has exceeded the drinking water standard (0.1 mg/l) during summers since 2006. Previous studies have found that temperature stratification occurred during summer, and anoxic hypolimnion developed where the water depth exceeded 8 m. However, water temperature stratification did not occur in areas where the water depth was less than 8 m. Soluble Mn(II) was found in the anoxic hypolimnion, but no Mn(II) was found in the shallow water (less than 8 m). Little manganese was found in the inflow water, but the sediments were found to be rich in manganese (Chen et al. 2015). This observation indicates that the dominant source of Mn(II) to the hypolimnion was most likely the reduction of manganese oxides in the sediments. Therefore, manganese in the sediments is

released when the thermocline occurs during summer in areas where water depth is greater than 8 m.

Methodology

Numerical model description

CE-QUAL-W2 model

The development of the numerical model was based on the CE-QUAL-W2 model. CE-QUAL-W2 is a two-dimensional (longitudinal and vertical), horizontally averaged water dynamics and water quality simulation software (Chung and Gu 1998). The current version of the model does not have a manganese module. We added a manganese geochemical module to the model to simulate manganese pollution. The reasons why we choose CE-QUAL-W2 include the following: (1) the model has been developed over more than 30 years with hundreds of successful applications in many countries, rendering it suitable for modeling reservoirs, lakes, rivers, and estuaries; (2) CE-QUAL-W2 assumes that the horizontal flow condition is constant, which grants high efficiency and is particularly suitable for relatively long and narrow water bodies, such as the Wangjuan reservoir; (3) the model is open source and has detailed information for users, especially for new function developers; and (4) the model is effective at simulating water temperature stratification, which is a key process for manganese pollution (Yu et al. 2010). Additionally, CE-QUAL-W2 can simulate the water surface elevation, velocity, temperature, 21 water quality parameters, and more than 60

other related variables. The fundamental equations of CE-QUAL-W2 are documented by Cole and Wells (2013).

Model modification

In this study, manganese geochemical reactions were added to the CE-QUAL-W2 model. The Mn cycle consists of two species: a reduced form, Mn(II), and an oxidized form, Mn(IV) oxide (referred to as particulate Mn or Mn_p). Mn(II) is derived from Mn in the sediment, and high concentrations of Mn(II) appear in the hypolimnion and migrate to upper water levels by convection diffusion (Yagi 1996). Mn(II) can be removed from the water by oxidation, absorption on colloidal material, and precipitation. In this model, only the first process is included because the last two have limited effects. The settling of Mn oxide is assumed to occur at a uniform rate throughout the water column. The detailed calculation method is as follows:

Mn(II) oxidation with oxygen in water:

$$2Mn^{2+} + O_2 + 2H_2O \rightarrow 2MnO_2 + 4H^+ \qquad (1)$$
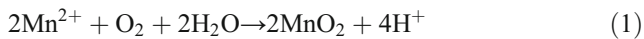
The rate of this process depends on the concentrations of both Mn(II) and O_2:

$$r = K_{om}[O2]\left[Mn^{2+}\right] \qquad (2)$$

where the reaction rate constant K_{om} refers to the measurement value in the literature (Lopes et al. 2010).

The flux of Mn(II) from the sediment is simulated by using a function of the sediment oxygen demand, temperature, and release rate constant, whose threshold value is limited by the dissolved oxygen content.

$$Mn_{release} = Mnr*SODD*(1-[O2]/([O2] + KDO) \qquad (3)$$

where $Mn_{release}$ is the release rate of manganese (g/m^3/s); Mnr is the release rate constant; SODD is the sediment oxygen demand (g/m^2/day), which is a function of the temperature and interaction area; and KDO is the half-saturated concentration of oxygen (g/m^3).

Model setup

The Wangjuan reservoir was divided according to the topographic map into 38×35 (longitudinal × vertical) rectangular grids with grid longitudinal lengths of 100–400 m and a vertical length of 0.5 m. The reservoir has four branches; the no. 1 branch is from the inflow of the Lianyin River into the dam. The horizontal width of each grid was taken from the topographic map. Finally, the grid generation was calibrated according to the water level–capacity curve. The reservoir grids are shown in Fig. 2.

The inflow of the Wangjuan reservoir was the discharge of the Lianyin River. The upstream boundary conditions included inflow discharge and water temperature. The inflow discharge was calculated according to the rainfall and runoff coefficients of the region and modified based on the reservoir water level monitoring data. The inflow water temperature was calculated based on Groeger and Bass's (2005) formula. The Wangjuan reservoir has a water tunnel and a spillway. No flood discharge occurred during the simulated time, so the spillway was not used. The downstream boundary conditions comprised the discharge in the water tunnel, which was provided by the reservoir control office. The surface boundary conditions included heat exchange, which was affected by meteorological conditions such as the temperature, dew point temperature, wind speed and direction, cloud cover, and solar radiation. Meteorological data from nearby weather stations were downloaded from the Chinese meteorological data-sharing network. The bottom boundary condition was assumed to be impermeable without exchange between the reservoir and the groundwater. The heat exchange between the sediments and the bottom water was calculated by using three parameters: the sediment temperature, water temperature, and heat exchange coefficient.

The simulations in this study began on July 6, 2011. The initial water level was the measured water level on that day. The initial vertical profiles of temperature, TDS, ammonia nitrogen, nitrate, dissolved oxygen, and phosphate concentration were created from the measured data.

Model calibration

Calibration is an important process in water quality model development (Zhao et al. 2013). Model calibration for this study was implemented in two steps: the hydrodynamic part was calibrated first; then, the water quality part was activated and calibrated. The model parameters were iteratively changed by using a trial and error approach until the simulations led to qualitative agreement with the measurements. The hydrodynamic calibration included the water level and water temperature, while the water quality calibration included the dissolved oxygen and Mn(II).

The water level was calibrated for the period from July 6, 2011, to December 30, 2011. The measured water level data were received from the reservoir control office. The simulated water level agreed well with the measured water level (Fig. 3). The simulation error was less than 0.5 %, and the root mean square error was 0.02.

After the flow balance was verified, the hydrodynamic part was further calibrated by using measured water temperature data. The water temperature was calibrated between the simulated and measured vertical profiles in the deepest point of the reservoir near the dam on August 18, September 7, and November 1, 2011. On August 18, the measured results
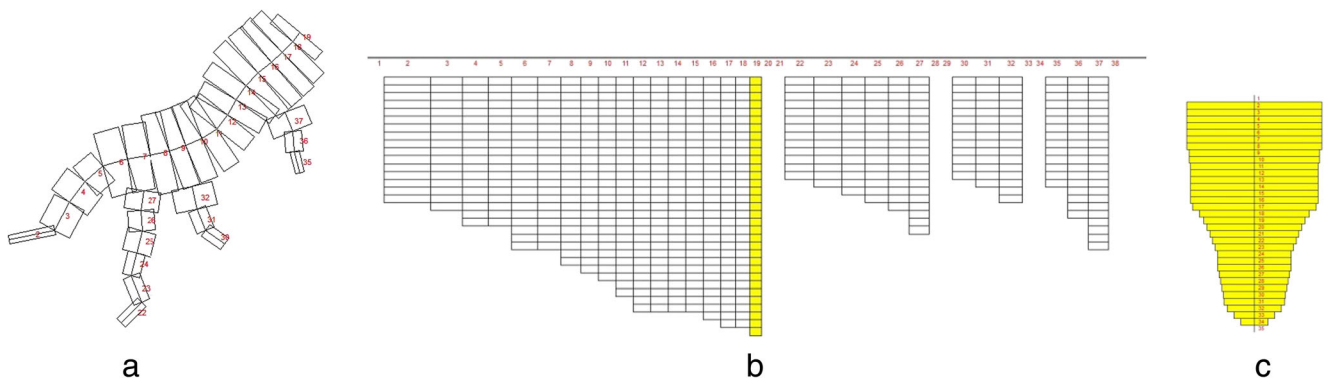
Fig. 2 Partitioning of the reservoir: **a** plan view; **b** longitudinal profiles; and **c** segment sections

showed that the water temperature began to decline at a depth of 5 m, and the water temperature at 11 m depth was 7 °C lower than the surface water temperature. On September 7, small differences were present between the bottom water temperature and the surface water temperature. On November 1, the reservoir water temperatures of every layer were consistent, with no temperature changes. Thus, reservoir water temperature stratification existed in August and started to abate in September before completely disappearing. This comparison showed that the model could successfully reproduce the spatial and temporal variability of the water temperature during the thermal stratification process (Fig. 4). Both the water level and water temperature calibration results suggest that the model can reasonably represent the hydrodynamic processes in the reservoir, hence forming a foundation to further calibrate water quality processes.

The dissolved oxygen (DO) was calibrated before the Mn(II) because the DO is an important variable for Mn(II) simulations. The DO was calibrated between the simulated and measured vertical profiles at the deepest point of the reservoir near the dam on August 18, September 7, and November 1, 2011. On August 18, the measurements showed that the DO displayed a decreasing trend from the surface to

the bottom. On September 7, the DO changed slightly from the surface water to a depth of 10 m, but the DO below this 10 m depth was obviously smaller than the upper values. On November 1, the DO values showed no vertical differences. Thus, the DO deficit of the hypolimnion occurred in August and began to abate in September, but no DO deficit existed in November. The general trends were, at least qualitatively, reproduced by the simulation (Fig. 5). On August 18, the simulated DOs in the hypolimnion were smaller than the measured ones, which may have been caused by aeration in the sampling.

The Mn(II) was calibrated between the simulated and measured vertical profiles in the deepest point of the reservoir near the dam on August 18 and September 7, 2011. On November 1, Mn(II) was not detected. On August 18, the monitoring results showed that Mn(II) was absent from the surface to a depth of 9 m but existed at greater depths. On September 7, Mn(II) was absent from the surface to a depth of 10 m but existed at greater depths. Thus, Mn(II) appeared in the hypolimnion in August and began to abate in September but disappeared in November. The simulated Mn(II) matched the measured data well in the vertical profile (Fig. 6), which confirms that the model successfully simulated the manganese pollution.
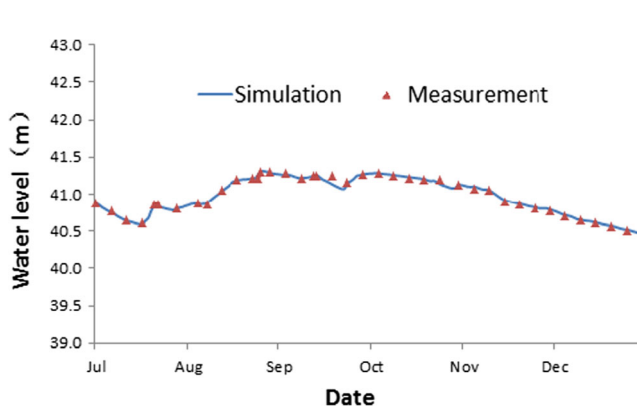

Fig. 3 Comparison of simulated and measured water levels from July 6 to Dec 31, 2011. Points represent the measured values; lines delineate the model simulation
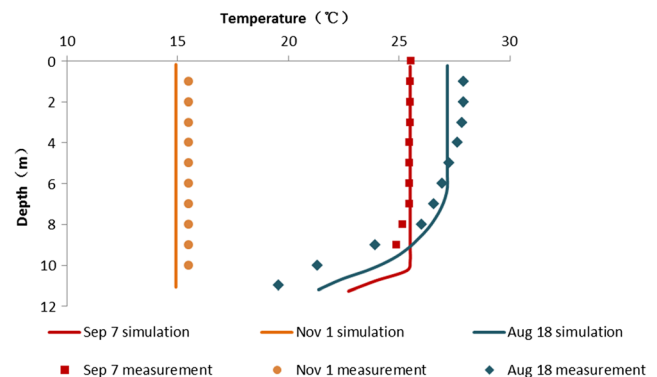

Fig. 4 Comparison of simulated and measured vertical water temperature profiles on August 18, September 7, and December 1, 2011, at the deepest point of the reservoir. *Points* represent measured values; *lines* delineate model simulations
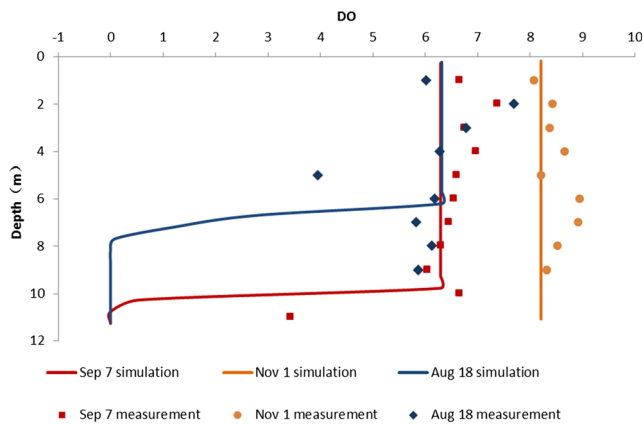
Fig. 5 Comparison of simulated and measured DO vertical profiles on August 18, September 7, and December 1, 2011, at the deepest point of the reservoir. *Points* represent measured values; *lines* delineate model simulation

The most important features of the measured profiles were been simulated by the model. Hence, the model can be used for water temperature stratification and manganese pollution simulations in the Wangjuan reservoir.

Model application

The calibrated model was applied to investigate the impacts of environmental factors on water temperature stratification and manganese pollution. A series of numerical experiments (15 cases, Table 1) were conducted with different input values of air temperature, water level, wind speed, and wind direction. Case 1 was the baseline, which used the measured data from July 6, 2011, to July 6, 2012. Cases 2 and 3 were high and low air temperature scenarios, with air temperature inputs that were 5 °C higher and lower than the measured temperature, respectively. Cases 4 and 5 were high and low water level scenarios, with initial water levels that were 2 m higher and lower than the measured water level, respectively. Cases 6 and
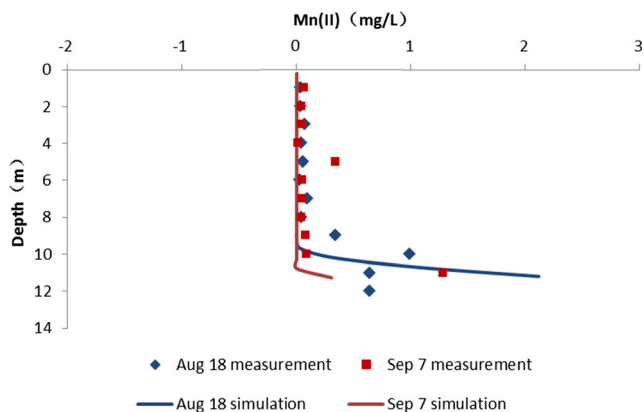

Fig. 6 Comparison of simulated and measured Mn(II) vertical profiles on August 18 and September 7, 2011, at the deepest point of the reservoir. *Points* represent measured values; *lines* delineate model simulations

7 were high and low wind speed scenarios, with wind speeds that were 0.5 m/s higher and lower than the measured wind speed, respectively. Cases 8–15 were a group of wind direction scenarios. The wind directions in cases 8–15 were north (N), northeast (NE), east (E), southeast (SE), south (S), southwest (SW), west (W), and northwest (NW), respectively.

Results

Temporal variation in manganese pollution

The model can also provide continuous representations of the water temperature and Mn(II) concentrations. The changes in the water temperature and Mn(II) concentrations over time were analyzed before examining the influencing factors of manganese pollution. We conducted a simulation from July 6, 2011, to July 5, 2012. The simulation results (Fig. 7) showed that the upper water temperatures from early July to early September were greater than the bottom water temperature, thus demonstrating water temperature stratification. During this water temperature stratification period, the bottom water temperature was stable, but the upper water temperature began to decline in late August and reached levels that were close to the bottom water temperature in early September, ending the water temperature stratification. In the next year, the water temperature difference between the surface and bottom appeared in early May. The difference became large with time. Therefore, water temperature stratification started in early May and developed in May and June.

Figure 6 shows that the Mn(II) concentration changed over time at the bottom of the reservoir near the dam (at 11 m depth). Manganese pollution started in mid-July, with concentrations gradually increasing to a maximum of approximately 2 mg/l on August 20. From August 20 to early September, the Mn(II) concentrations reduced sharply before finally disappearing completely. From September to the next June, no Mn(II) was present.

The results showed that the manganese pollution reached its maximum level around August 20. Therefore, attention was paid to both the distribution of the water temperature stratification and the manganese pollution on August 20 in the following analysis.

Impacts of air temperature

The results of cases 2 and 3 (Table 1) were compared to those of Case 1 to assess the impact of air temperature on manganese pollution. The water temperature longitudinal profiles on August 20, 2011, were selected to reflect the water temperature stratification (Fig. 8). In case 2, an obvious increase in the upper water temperature was present compared to case 1: the water temperature difference between the upper water and

Table 1 Model simulation scenarios

	Air temperature	Water level	Wind speed	Wind direction
Case 1	The measured temperature	The initial water level of 40.9 m	The measured wind speed	The measured wind direction
Case 2	5 °C higher than the measured temperature			The measured wind direction
Case 3	5 °C lower than the measured temperature			The measured wind direction
Case 4		The initial water level of 42.9 m		The measured wind direction
Case 5		The initial water level of 38.9 m		The measured wind direction
Case 6			0.5 m/s greater than the measured wind speed	The measured wind direction
Case 7			0.5 m/s slower than the measured wind speed	The measured wind direction
Cases 8–15				Wind directions of N, NE, E, SE, S, SW, W, and NW, respectively

bottom water increased. In case 3, the water temperature stratification disappeared. The water temperatures of the upper water and bottom water were the same. The areas of Mn(II) concentrations above 0.1 mg/l on August 20, 2011, were selected to reflect the range of manganese pollution (Fig. 9). In case 2, the area of Mn(II) concentration above 0.1 mg/l increased compared to case 1. In case 3, the area of Mn(II) concentration above 0.1 mg/l almost disappeared. The Mn(II) longitudinal profiles on August 20, 2011 were selected to reflect the vertical distribution of manganese pollution (Fig. 10). In case 2, the thickness of the Mn(II) area increased by approximately 0.8 m compared to case 1. In case 3, Mn(II) only existed in the deepest water area.

Impacts of water level

The results of cases 4 and 5 (Table 1) were compared to those of case 1 to assess the impact of water level on manganese pollution. The water temperature longitudinal profiles on
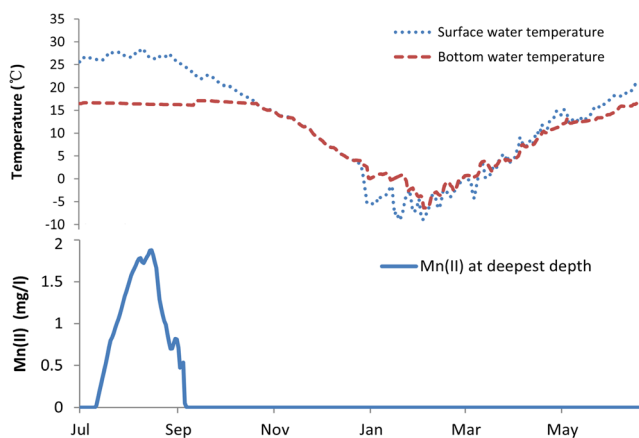

Fig. 7 Simulated water temperature at the surface and bottom, and Mn(II) concentrations at the bottom of the deepest point of the reservoir from July 6, 2011, to July 5, 2012

August 20, 2011, are shown in Fig. 8. The results demonstrated that the water level greatly influenced the water temperature. In case 4, the thermocline rose by approximately 2 m, and the hypolimnion's thickness increased. In case 5, the bottom temperature increased significantly. The area of Mn(II) concentration above 0.1 mg/l on August 20, 2011, is shown in Fig. 9. In case 4, the area of Mn(II) above 0.1 mg/l expanded. In case 5, the range of Mn(II) above 0.1 mg/l almost disappeared. The Mn(II) longitudinal profiles on August 20, 2011, are shown in Fig. 10. In case 4, the thickness of the Mn(II) area increased. The upper boundary of the Mn(II) rose by approximately 2.5 m. In case 5, Mn(II) almost disappeared; only the deepest areas near the dam had small quantities of Mn(II).

Impacts of wind speed

The results of cases 6 and 7 (Table 1) were compared to those of case 1 to assess the impact of wind speed on manganese pollution. The results demonstrated that the wind speed greatly influenced the water temperature and manganese pollution. The water temperature longitudinal profiles on August 20, 2011, are shown in Fig. 8. In case 6, the hypolimnion thickness increased. In case 7, the bottom temperature increased significantly, and the water temperature was uniform. No water temperature stratification occurred. The area of Mn(II) concentration above 0.1 mg/l on August 20, 2011, is shown in Fig. 9. In case 6, the area of Mn(II) above 0.1 mg/l increased. In case 7, the area of Mn(II) above 0.1 mg/l almost disappeared. The Mn(II) longitudinal profiles on August 20, 2011, are shown in Fig. 10. In case 6, the thickness of the Mn(II) area increased. The upper boundary of the Mn(II) rose by approximately 2 m. In case 7, only the deepest areas near the dam had small amounts of Mn(II).
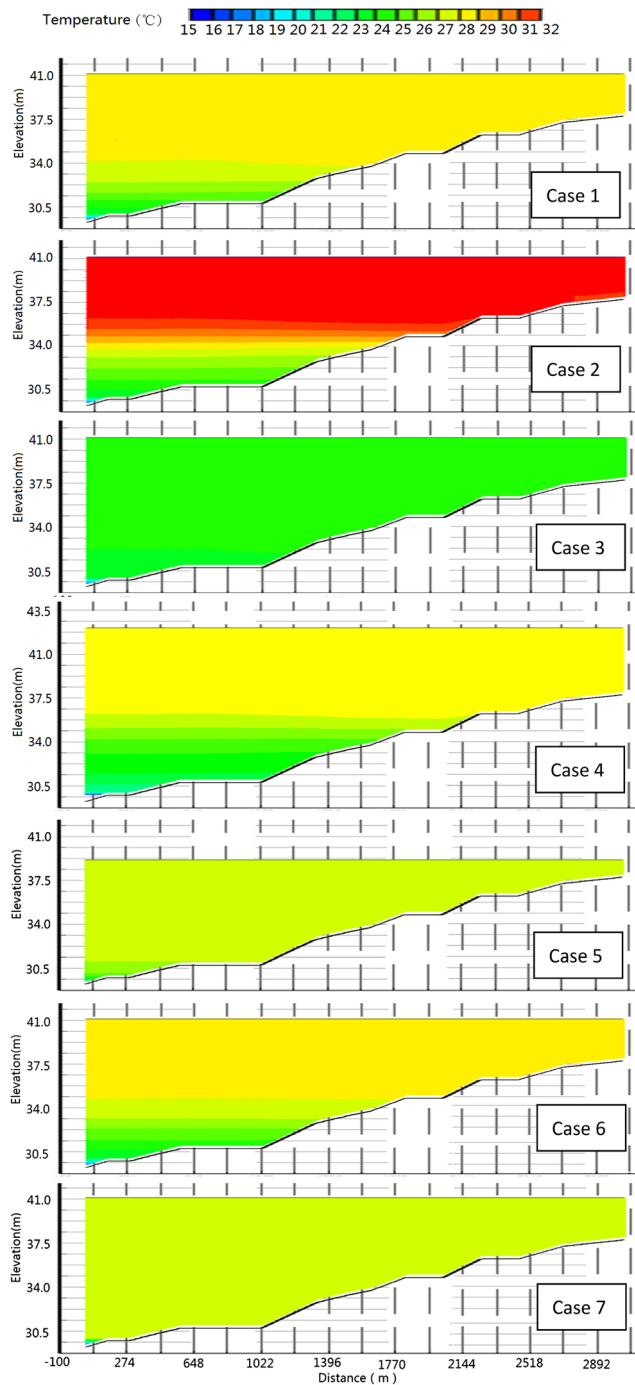
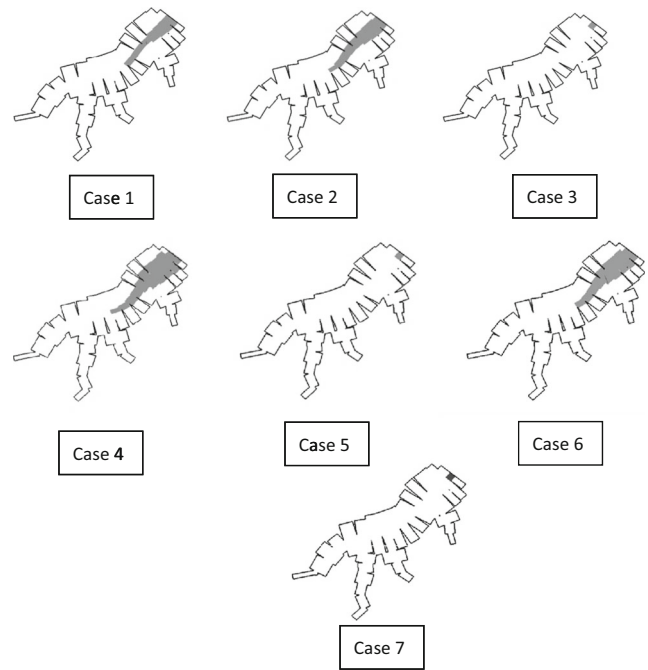**Fig. 8** Simulated water temperature longitudinal profiles for cases 1–7

Fig. 9 Area of simulated manganese that exceeded 0.1 mg/l for cases 1–7

Mn(II) concentration for the S wind direction is only 0.57 mg/l. No Mn(II) was recorded for the SW and W wind directions. For the W wind direction, the water temperature difference between the surface and bottom decreased after the beginning of the simulation and finally disappeared in August (Fig. 12). The flow of the reservoir was from SW to NE, which meant that the W, SW, and S wind directions had the same direction as the flow. These wind directions made the water stratification disappear, thus preventing manganese pollution. On the contrary, the NE wind direction, which was opposite to the flow direction, aggravated manganese pollution.

Discussion

The simulation results for changes in the water temperature stratification and manganese pollution over time showed that manganese pollution occurs after water temperature stratification appears. When water temperature stratification abates, manganese pollution disappears. Therefore, manganese pollution in reservoirs is directly related to water temperature stratification. Previous studies (Atkinson et al. 2007; Pakhomova et al. 2007; Graham et al. 2012) found that manganese pollution is caused by water temperature stratification and dissolved oxygen deficits in the hypolimnion, which is consistent with our simulation results. Therefore, the influencing factors of water temperature stratification in reservoirs, including the temperature, water level, wind speed, and wind direction, impact the process of manganese pollution.
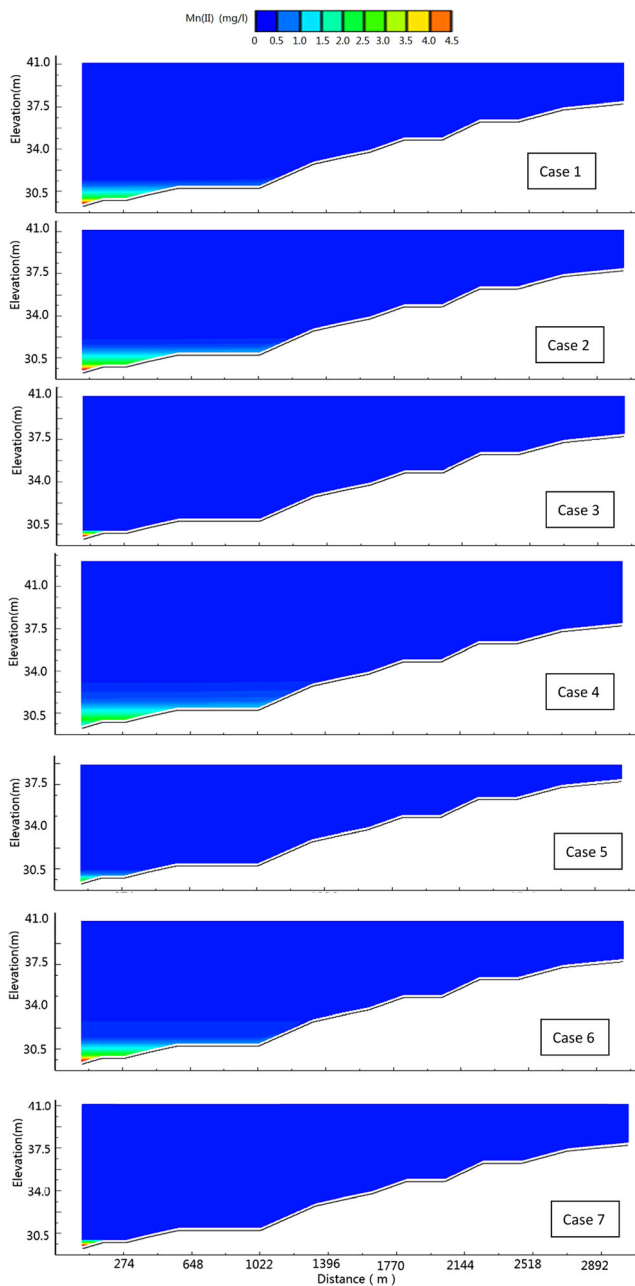
Impacts of wind direction

The maximum Mn(II) concentration at the bottom of the deepest depth was chosen as the index to assess the impact of wind direction on manganese pollution. The maximum Mn(II) concentrations for cases 8–15 (Table 1) are shown in Fig. 11. The maximum Mn(II) concentrations for the NW, N, NE, E, and SE wind directions are approximately 1.8 mg/l, with the largest value in the NE direction. The maximum

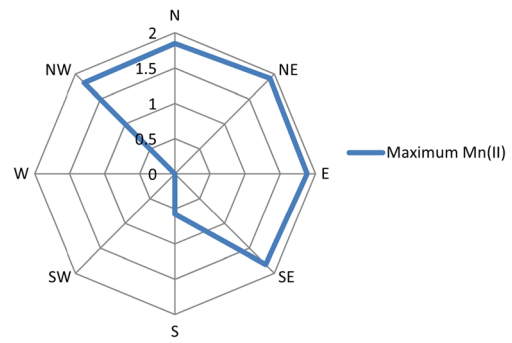Fig. 10 Simulated Mn(II) longitudinal profiles for cases 1–7

Fig. 11 Simulated maximum Mn(II) concentrations at the bottom of the deepest point of the reservoir for different wind direction cases

drops, manganese pollution almost disappears and Mn(II) concentrations decrease. This result is consistent with the observations that were discussed above. The concentrations of manganese in shallow water are small because water temperature stratification does not exist.

The wind speed also greatly influences the water temperature and manganese pollution. Greater wind speed decreases water temperature stratification and causes manganese pollution to almost disappear. This result demonstrates that the wind speed accelerates water mixing between the top and bottom and increases the transmission of dissolved oxygen downward. Lower wind speed causes manganese pollution to expand, as the downward transport of dissolved oxygen decreases and the oxygen deficit in the hypolimnion is aggravated.

Different wind directions have different impacts on manganese pollution. Wind that travels in the same direction as the flow reduces manganese pollution, while wind that travels in the opposite direction of the flow aggravates manganese pollution. During summer, SE is the predominant wind direction in this reservoir. This wind direction does not reduce manganese pollution according to our results.

The simulation results show that the air temperature, water level, wind speed, and wind direction have important influences on manganese pollution. When high air temperatures, high water levels, small wind speeds, or wind in the opposite direction as the flow occur, reservoir management departments should issue early warnings for manganese pollution and prepare to take corresponding control measures. Because manganese pollution mainly appears

The air temperature directly affects the upper water temperature, but its impact on the bottom water temperature is limited. Hence, the bottom water temperature is not affected by changes in the air temperature. Higher air temperatures increase the upper water temperatures and causes manganese pollution in reservoirs to expand and worsen. In contrast, lower air temperature causes water temperature stratification, and thus manganese pollution, to disappear.

The water level can greatly influence the water temperature and manganese pollution. Increasing water level causes manganese pollution to expand, which may be caused by greater oxygen deficits in the hypolimnion. When the water level
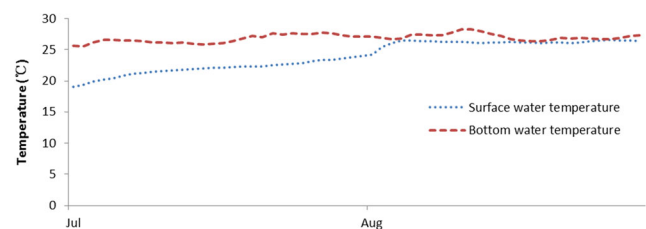

Fig. 12 Simulated water temperature at the surface and bottom in July and August of the W wind direction

in deeper water areas, this phenomenon could be eliminated by physical or chemical methods. Water temperature stratification or oxygen deficits in hypolimnion could be eliminated by means of aeration devices or the addition of antioxidants.

Conclusions

This study developed a reservoir manganese pollution numerical model by adding a manganese biogeochemical module to the two-dimensional water quality software CE-QUAL-W2. The Wangjuan reservoir was used as an example to simulate the hydrodynamic and water quality processes while focusing on the formation of manganese pollution during summer and autumn. In this study, experimental data were used to verify the model, including the water level, the water temperature, the dissolved oxygen, and the Mn(II) concentrations. The model was able to reproduce all the above distributions with reasonably good accuracy. After verification, the model was used to simulate different scenarios of air temperature, water level, wind speed, and wind direction. The simulation results showed that high air temperature, high water level, and low wind speed increased manganese pollution, while low air temperature, low water level, and high wind speed decreased manganese pollution. Wind in the same direction as the flow reduced manganese pollution, while wind in the opposite direction of the flow aggravated manganese pollution.

References

Abesser C, Robinson R, Robinson R (2010) Mobilisation of iron and manganese from sediments of a Scottish Upland reservoir. J Limnol. doi:10.4081/jlimnol.2010.42

Atkinson CA, Jolley DF, Simpson SL (2007) Effect of overlying water pH, dissolved oxygen, salinity and sediment disturbances on metal release and sequestration from metal contaminated marine sediments. Chemosphere 69:1428–1437. doi:10.1016/j.chemosphere.2007.04.068

Baden SP, Eriksson SP, Weeks JM (1995) Uptake, accumulation and regulation of manganese during experimental hypoxia and normoxia by the decapod Nephrops norvegicus (L.). Mar Pollut Bull 31:93–102. doi:10.1016/0025-326X(94)00257-A

Bryant CL, Farmer JG, MacKenzie AB et al (1997) Manganese behavior in the sediments of diverse Scottish freshwater lochs. Limnol Oceanogr 42:918–929. doi:10.4319/lo.1997.42.5.0918

Bryant LD, Hsu-Kim H, Gantzer PA, Little JC (2011) Solving the problem at the source: controlling Mn release at the sediment-water interface via hypolimnetic oxygenation. Water Res 45:6381–6392. doi:10.1016/j.watres.2011.09.030

Castelletti A, Pianosi F, Soncini-Sessa R, Antenucci JP (2010) A multiobjective response surface approach for improved water quality planning in lakes and reservoirs. Water Resour Res 46:1–16. doi:10.1029/2009WR008389

Chen L, Zheng X, Wang T, Zhang J (2015) Influences of key factors on manganese release from soil of a reservoir shore. Environ Sci Pollut Res 22:11801–11812. doi:10.1007/s11356-015-4443-5

Chung S, Gu R (1998) Two-dimensional simulations of contaminant currents in stratified reservoir. J Hydraul Eng 124:704–711. doi:10.1061/(ASCE)0733-9429(1998)124:7(704)

Cole TM, Wells SA (2013) CE-QUAL-W2: a two-dimensional, laterally averaged, hydrodynamic and water quality model, version 3.71. Portland State University, Portland

Farmer JG, Lovell MA (1984) Massive diagenetic enhancement of manganese in Loch Lomond sediments. Environ Technol Lett 5:257–262. doi:10.1080/09593338409384274

Gantzer PA, Bryant LD, Little JC (2009) Controlling soluble iron and manganese in a water-supply reservoir using hypolimnetic oxygenation. Water Res 43:1285–1294. doi:10.1016/j.watres.2008.12.019

Graham MC, Gavin KG, Kirika A, Farmer JG (2012) Processes controlling manganese distributions and associations in organic-rich freshwater aquatic systems: the example of Loch Bradan, Scotland. Sci Total Environ 424:239–250. doi:10.1016/j.scitotenv.2012.02.028

Groeger AW, Bass DA (2005) Empirical predictions of water temperatures in a subtropical reservoir. Arch Für Hydrobiol 162:267–285. doi:10.1127/0003-9136/2005/0162-0267

Hamilton-Taylor J, Davison W, Morfett K (1996) The biogeochemical cycling of Zn, Cu, Fe, Mn and dissolved organic C in a seasonally anoxic lake. Limnol Oceanogr 41:408–418

Johnson CA, Ulrich M, Sigg L, Imboden DM (1991) A mathematical model of the manganese cycle in a seasonally anoxic lake. Limnol Oceanogr 36:1415–1426

Kohl PM, Medlar SJ (2006) Occurrence of manganese in drinking water and manganese control. AWWA and USEPA. IWA Publishing, Philadelphia

Kristiansen KD, Kristensen E, Jensen EMH (2002) The influence of water column hypoxia on the behaviour of manganese and iron in sandy coastal marine sediment. Estuar Coast Shelf Sci 55:645–654. doi:10.1006/ecss.2001.0934

Löfgren S, Boström B (1989) Interstitial water concentrations of phosphorus, iron and manganese in a shallow, eutrophic swedish lake—implications for phosphorus cycling. Water Res 23:1115–1125. doi:10.1016/0043-1354(89)90155-3

Lopes FA, Michard G, Poulin M et al (2010) Biogeochemical modelling of a seasonally anoxic lake: calibration of successive and competitive pathways and processes in Lake Aydat, France. Aquat Geochem 16:587–610. doi:10.1007/s10498-010-9095-y

Miao S, DeLaune RD, Jugsujinda A (2006) Influence of sediment redox conditions on release/solubility of metals and nutrients in a Louisiana Mississippi River deltaic plain freshwater lake. Sci Total Environ 371:334–343. doi:10.1016/j.scitotenv.2006.07.027

Pakhomova SV, Hall POJ, Kononets MY et al (2007) Fluxes of iron and manganese across the sediment–water interface under various redox conditions. Mar Chem 107:319–331. doi:10.1016/j.marchem.2007.06.001

Roitz JS, Flegal AR, Bruland KW (2002) The biogeochemical cycling of manganese in San Francisco Bay: temporal and spatial variations in surface water concentrations. Estuar Coast Shelf Sci 54:227–239. doi:10.1006/ecss.2000.0839

Sakata M (1985) Diagenetic remobilization of manganese, iron, copper and lead in anoxic sediment of a freshwater pond. Water Res 19:1033–1038. doi:10.1016/0043-1354(85)90373-2

Stauffer RE (1993) Effects of an early fall cold front on heat, phosphorus, silica, and manganese distributions in the hypolimnion of Lake Mendota, Wisconsin. J Hydrol 151:1–18. doi:10.1016/0022-1694(93)90245-5

Sundby B, Anderson LG, Hall POJ et al (1986) The effect of oxygen on release and uptake of cobalt, manganese, iron and phosphate at the sediment-water interface. Geochim Cosmochim Acta 50:1281–1288. doi:10.1016/0016-7037(86)90411-4

World Health Organisation (2011) Guidelines for drinking. Water Quality, Geneva

Yagi A (1996) Manganese flux associated with dissolved and suspended manganese forms in Lake Fukami-ike. Water Res 30:1823–1832. doi:10.1016/0043-1354(96)00073-5

Yu SJ, Lee JY, Ha SR (2010) Effect of a seasonal diffuse pollution migration on natural organic matter behavior in a stratified dam reservoir. J Environ Sci 22:908–914. doi:10.1016/S1001-0742(09)60197-2

Zaw M, Chiswell B (1999) Iron and manganese dynamics in lake water. Water Res 33:1900–1910. doi:10.1016/S0043-1354(98)00360-1

Zhao L, Li Y, Zou R et al (2013) A three-dimensional water quality modeling approach for exploring the eutrophication responses to load reduction scenarios in Lake Yilong (China). Environ Pollut 177:13–21. doi:10.1016/j.envpol.2013.01.047